Spherical and cylindrical nucleation centers in a bulk ferromagnet

Amikam Aharoni* and W. Baltensperger
Theoretische Physik, Eidgenössische Technische Hochschule Hönggerberg, CH-8093 Zürich, Switzerland
(Received 23 October 1991)

The process of nucleation of magnetization reversal in bulk materials, by creating pairs of one-dimensional, planar Bloch or Néel walls, is extended here to the creation of spherical or cylindrical nuclei. Numerical integration of the appropriate differential equation leads to a saddle point in energy, which gives the barrier to be overcome for reversing the magnetization. The results for both cases are rather similar to the planar ones, but for vanishingly small fields the energy of the nucleus of a reversal structure tends to *infinity*, which means that it takes some finite field for any reversal to nucleate.

I. INTRODUCTION

Magnetization reversal by domain-wall motion is a rather slow process. The process of nucleation of a pair of Bloch or Néel walls[1] showed some promise[2] as a sufficiently fast mechanism, but it was not possible to evaluate the time dependence in a wall with planar symmetry: It involves an infinite energy in an infinite material (even though the energy per unit length is always finite everywhere), for *any* value of the applied field.

The present study presents a similar nucleation structure for a spherical or a cylindrical nucleation center. Its energy also diverges for zero applied field, which makes it theoretically impossible to reverse the magnetization of *any* ferromagnet unless some field is applied. This result is not surprising, because it implies the stability of the ferromagnetic state, without an applied field, in an infinitely large volume. However, for any *finite* field the total energy barrier for the spherical nucleus (unlike that for the planar or cylindrical center) is finite, which should make it possible to estimate reversal times on a more realistic basis than was ever done before.

For the spherical nucleation center we assume a magnetization which depends only on the radial coordinate, in an infinite material. We have not tried to consider any nucleation modes that have an angle dependence. In case there exists a mode for which the energy barrier is smaller than that calculated here, the present calculation leads to an upper bound for the smallest possible energy barrier. Similarly, we assume a dependence on the cylindrical radial coordinate only, for the case of a cylindrical nucleation center, and the same limitations apply to this case as well.

The spherical nucleus is meant to be an approximation to the more realistic nucleation processes at crystalline point defects, but the details of the defect itself are not considered in this study. Similarly, the cylindrical nucleation center is meant to be a crude representation of nucleation around the dislocation lines, but again the actual effect of these dislocations is neglected here.

II. SPHERICAL NUCLEUS

A. General

Consider a large spherical particle, whose radius is R (which will later be taken in the limit $R \rightarrow \infty$). Let it be made of a ferromagnetic material with a uniaxial anisotropy, whose anisotropy constant is K_u. Let the magnetization vector in this sphere be expressed in terms of a single function of space ω, so that

$$M_x = M_s \sin\omega, \quad M_y = 0, \quad M_z = M_s \cos\omega, \tag{1}$$

where M_s is the saturation magnetization, and where ω is assumed to be a function of the spherical coordinate r only. The magnetization thus lies in the xz plane, at an angle ω to the z axis, which gradually approaches π for large r. It should be noted that the assumption that ω depends only on r is arbitrary, and does not guarantee that the lowest possible energy barrier is obtained.

The exchange energy of this structure is

$$W_e = \frac{C}{2}\int[(\nabla \sin\omega)^2 + (\nabla \cos\omega)^2]\, dV, \tag{2}$$

where $C(=2A)$ is the exchange constant, and where the integration is over the sphere. Hence

$$W_e = \frac{C}{2}\int\left(\frac{d\omega}{dr}\right)^2 dV. \tag{3}$$

In order to simplify the notation, the energy terms here will be normalized to the energy

$$W_0 = 8\pi C^{3/2}/(2K_u)^{1/2}, \tag{4}$$

while length will be expressed in terms of the reduced parameter,

$$t = r\sqrt{2K_u/C}. \tag{5}$$

In Co, for example, $C = 2.6 \times 10^{-6}$ erg/cm and $K_u = 4.3 \times 10^6$ erg/cm^3,[3] so that our unit for the energy is $W_0 = 3.6 \times 10^{-11}$ erg, and the normalization of length is in units of about 5.5 nm.

When this notation is used in Eq. (3), and the integrations over the angles are carried out, the reduced exchange energy term becomes for the limit of $R \to \infty$,

$$\mathcal{E}_e = \frac{W_e}{W_0} = \frac{1}{4}\int_0^\infty t^2 \left(\frac{d\omega}{dt}\right)^2 dt. \tag{6}$$

Similarly, the anisotropy energy term, normalized by the same factor, is

$$\mathcal{E}_a = \frac{W_a}{W_0} = \frac{1}{4}\int_0^\infty t^2 \sin^2\omega\, dt. \tag{7}$$

Let a magnetic field H_z be applied along the $+z$ direction. The reduced energy *difference* between the interaction of the configuration of Eq. (1) with this field, and the interaction of a sphere saturated in the $-z$ direction with the same field is

$$\mathcal{E}_f = \frac{W_f}{W_0} = -\frac{h}{2}\int_0^\infty t^2(1+\cos\omega)\, dt = -h\mathcal{M}, \tag{8}$$

where

$$h = H_z M_s/(2K_u). \tag{9}$$

In the case of Co, with[3] $M_s = 1422$ emu, the unit of h corresponds to 6 kOe.

To these terms one should add the magnetostatic self-energy term. However, the contribution of the volume charge just cancels that of the surface charge, and the total magnetostatic energy is exactly the same as in the *saturated* sphere. This equality has been noted[4] for a particular form of rotation of a small sphere at the center of a large sphere. It is proved in the Appendix to be a general property of the magnetization structure studied here, with ω a function of r only. Since only the energy difference from the saturated state is considered, it is zero for this energy term. In comparing with experiments on crystals with a real surface, the magnetostatic term is naturally included by taking H_z in Eq. (9) to be the internal field.

Neglecting the effect of possible imperfections[5] and of an incomplete saturation,[6] the total energy to be considered is

$$\mathcal{E} = \mathcal{E}_e + \mathcal{E}_a + \mathcal{E}_f = \mathcal{E}_d - h\mathcal{M}. \tag{10}$$

The Euler differential equation which minimizes this total energy is

$$\frac{1}{t^2}\frac{d}{dt}\left(t^2\frac{d\omega}{dt}\right) - \frac{1}{2}\sin(2\omega) - h\sin\omega = 0, \tag{11}$$

with the boundary condition

$$d\omega/dt = 0 \tag{12}$$

at $r = R$, namely $t = \infty$. There is no *a priori* condition for $t = 0$, but it will be shown later from the properties of the differential equation (11) that Eq. (12) must also hold at $t = 0$.

In its linearized form, for $|\omega| \ll 1$, this equation is a particular case of the nucleation problem in a sphere, for which the solution is known.[7] In its nonlinear form no analytic solution is known, and a numerical solution had to be undertaken, as will be described in the following. However, since most of the previous calculations in the literature involve just a guess of a reversal mechanism, which is then modeled on a computer, it may be worth mentioning that we have also looked for a more conventional Ritz model, which will illustrate our present result. We have not been able to guess a variational function that leads to a saddle point.

B. Numerical integration

In the integration of Eq. (11), it is convenient to start from large values of t, for which the behavior can be expressed by the eigenfunctions of a *linear* differential equation. Consider first a more general case in which the solution of Eq. (11) is sought in the vicinity of a given value ω_0, namely for

$$\omega = \omega_0 + \epsilon, \tag{13}$$

and ϵ is small. Substituting this relation in Eq. (11) and neglecting higher than linear terms in ϵ,

$$\frac{1}{t^2}\frac{d}{dt}\left(t^2\frac{d\epsilon}{dt}\right) - \alpha^2\epsilon = A, \tag{14}$$

where

$$\alpha^2 = \cos(2\omega_0) + h\cos\omega_0, \tag{15a}$$

$$A = \tfrac{1}{2}\sin(2\omega_0) - h\sin\omega_0. \tag{15b}$$

It can be verified by substitution that

$$\epsilon = \frac{C_1 e^{\alpha t} + C_2 e^{-\alpha t}}{t} - \frac{A}{\alpha^2} \tag{15c}$$

is a solution of Eq. (14). It is also the most general solution because it contains two arbitrary constants, C_1 and C_2.

In particular, for very large t we are interested in the solution for which ω approaches π. Substituting $\omega_0 = \pi$ in Eqs. (15), it is seen that $A = 0$ and $\alpha = \sqrt{1-h}$. Also, C_1 must be zero for large t, or ω will diverge. Therefore, the solution in that region is

$$\omega = \pi - \frac{b}{t}e^{-t\sqrt{1-h}}, \tag{16a}$$

and its derivative is

$$\frac{d\omega}{dt} = b\left(\frac{\sqrt{1-h}}{t} + \frac{1}{t^2}\right)e^{-t\sqrt{1-h}}. \tag{16b}$$

In the other extreme, near the point $t = 0$, regularity requires that $C_1 = -C_2$ in Eq. (15c), whatever ω_0 is, which means

$$d\omega/dt = 0, \quad \text{for} \quad t = 0. \tag{17}$$

Therefore, the strategy used was to choose some T, and take Eqs. (16) as the solution for $t \geq T$, for a certain value of the parameter b. From the initial values of ω and its derivative at $t = T$, Eq. (11) was integrated numerically in about 1000 steps down to the vicinity of

$t = 0$. The value of b was then adjusted so as to fulfill Eq. (17). In some cases we made a plot of $\omega'(0)$ vs b, and the pattern was always the same: This derivative first increased from the value 0 at $b = 0$ [which corresponds to the trivial solution $\omega = \pi$ of Eq. (11)], then passed through a maximum, and decreased through 0. We have never encountered more than one zero in this process. The number of steps between $t = T$ and $t = 0$, as well as the value of T was varied to check convergence to the same results. Once $\omega(t)$ was thus found, the energy terms were computed numerically from Eqs. (6)–(8) for the region $t \leq T$. To the values thus obtained we added the contribution for the region $t \geq T$, taken as the first-order terms for small exponentials, namely

$$\begin{aligned}\mathcal{M}_L &= \frac{1}{2}\int_T^\infty t^2\left[1-\cos\left(\frac{b}{t}e^{-t\sqrt{1-h}}\right)\right]dt \\ &\approx \frac{b^2}{4}\int_T^\infty e^{-2t\sqrt{1-h}}dt \\ &= \frac{b^2 e^{-2T\sqrt{1-h}}}{8\sqrt{1-h}},\end{aligned} \tag{18}$$

$$\begin{aligned}\mathcal{E}_{d_L} &= \frac{1}{4}\int_T^\infty t^2\left[\left(\frac{d\omega}{dt}\right)^2+\sin^2\omega\right]dt \\ &\approx \frac{b^2}{4}\int_T^\infty\left(2-h+\frac{2\sqrt{1-h}}{t}+\frac{1}{t^2}\right)e^{-2t\sqrt{1-h}}dt \\ &= \frac{b^2}{4}\left(\frac{1}{T}+\frac{2-h}{2\sqrt{1-h}}\right)e^{-2T\sqrt{1-h}}.\end{aligned} \tag{19}$$

For the numerical integration of Eq. (11) it was usually sufficient to transform it to a difference equation. Nevertheless, a more accurate method was also used, mostly as a check of the less sophisticated standard method. To this end we use again Eq. (15c) in the vicinity of $\omega_0 = \omega(ma)$, for an integer m, where a is the integration step. The constants C_1 and C_2 are chosen so that both ω and its derivative pass continuously to their values for $t = ma$, thus leading to

$$\omega(t) = \omega(ma)+\frac{A}{\alpha^2}\left(\frac{ma}{t}\cosh\left[\alpha(t-ma)\right]-1\right)+\left(ma\omega'(ma)+\frac{A}{\alpha^2}\right)\frac{\sinh[\alpha(t-ma)]}{\alpha t}, \tag{20}$$

$$\omega'(t) = \left[ma\omega'(ma)+\frac{A}{\alpha^2}\left(1-\frac{ma}{t}\right)\right]\frac{\cosh[\alpha(ma-t)]}{t}+\left[\frac{ma}{t}\omega'(ma)+A\left(\frac{1}{\alpha^2 t}-ma\right)\right]\frac{\sinh[\alpha(ma-t)]}{\alpha t}, \tag{21}$$

where the prime designates the derivative. Substituting the particular value $t = (m-1)a$, expanding in powers of a, and taking the first nonvanishing term only,

$$\omega[(m-1)a] = \omega(ma)-\frac{ma}{m-1}\omega'(ma)+\frac{Aa^2}{2(m-1)}\left(m-\frac{1}{3}\right), \tag{22}$$

$$\omega'[(m-1)a] = \frac{m^2\omega'(ma)}{(m-1)^2}-\frac{Aa}{m-1}\left(m+\frac{1}{3(m-1)}\right). \tag{23}$$

Because of the factor $m-1$ in the denominator, this kind of iteration can be carried down to $m = 2$ only, so that the last value is the derivative at $t = a$, not $t = 0$. However, this last value is sufficient for aiming at Eq. (17), because this very equation proves that the derivative is *always* zero at the last point, $t = 0$, and the procedure has only to assure the continuity between $t = 0$ and $t = a$.

III. CYLINDRICAL NUCLEUS

A. General

We consider also the case of a reversal nucleus in the form of a circular (infinite) cylinder, instead of a sphere, along the same lines of the prèvious section. One case of this form is the curling mode[8] in a cylinder, in which M_ϕ is a function of ρ only, in a cylindrical coordinate system, ρ, z, ϕ. This form has been studied[9] already, and will not be repeated here. In this study we consider the same functional form as in Eq. (1), namely

$$M_\rho = M_s\sin\omega\cos\phi, \tag{24a}$$
$$M_\phi = -M_s\sin\omega\sin\phi, \tag{24b}$$
$$M_z = M_s\cos\omega, \tag{24c}$$

where now we take ω to be a function of ρ only, and the radius R is taken to be that of a large *cylinder*.

In order to calculate the magnetostatic energy term, we start from the potential

$$V_{\text{out}} = A(R/\rho)\cos\phi, \quad \text{for} \quad \rho \leq R \tag{25a}$$
$$V_{\text{in}} = A[f(\rho)/f(R)]\cos\phi, \quad \text{for} \quad \rho \leq R \tag{25b}$$

where A is a constant. It can be seen by substitution that this potential is continuous on $\rho = R$, and that it fulfills the differential equation

$$\nabla^2 V_{\text{out}} = 0. \tag{26}$$

It also satisfies

$$\nabla^2 V_{\text{in}} = 4\pi\nabla\cdot\mathbf{M}, \tag{27}$$

which in the present case is

$$\frac{4\pi}{\rho}\left(\frac{\partial}{\partial\rho}(\rho M_\rho)+\frac{\partial M_\phi}{\partial\phi}\right)=4\pi M_s\cos\phi\,\frac{d}{d\rho}[\sin\omega(\rho)], \tag{28}$$

provided

$$A\frac{f(\rho)}{f(R)}=\frac{4\pi M_s}{\rho}\int_0^\rho \rho'\sin\omega(\rho')\,d\rho'. \tag{29}$$

This equation also determines the constant A as

$$A=\frac{4\pi M_s}{R}\int_0^R \rho\sin\omega(\rho)\,d\rho, \tag{30}$$

and it is readily seen that the foregoing solution also fulfills the boundary condition,

$$\left(\frac{\partial V_{\rm in}}{\partial\rho}\right)_{\rho=R}-\left(\frac{\partial V_{\rm out}}{\partial\rho}\right)_{\rho=R}=4\pi(M_\rho)_{\rho=R}. \tag{31}$$

Since the magnetostatic problem can have only one solution for a given magnetization structure, the result

$$V_{\rm in}=\frac{4\pi M_s}{\rho}\cos\phi\int_0^\rho \rho'\sin\omega(\rho')\,d\rho' \tag{32}$$

is *the* solution of the potential problem.

The magnetostatic self-energy per unit length along z is

$$W_M=\frac{1}{2}\int_0^R\int_0^{2\pi}\mathbf{M}\cdot\nabla V_{\rm in}\,\rho\,d\phi\,d\rho. \tag{33}$$

Substituting from Eq. (32), and performing the integration over ϕ,

$$W_M=2\pi^2M_s^2\int_0^R\sin^2\omega(\rho)\,\rho\,d\rho, \tag{34}$$

which has the same *form* as that of the anisotropy energy. Actually, by using the notation

$$t=\rho\sqrt{\frac{2(K_u+\pi M_s^2)}{C}}, \tag{35a}$$

$$h=\frac{H_zM_s}{2(K_u+\pi M_s^2)}, \tag{35b}$$

all the energy terms become similar to those of the spherical case discussed in the foregoing. The *total* energy per unit length along z can then be written as

$$\mathcal{E}=W_{\rm total}/(\pi C)=\mathcal{E}_d-h\mathcal{M}, \tag{36}$$

with

$$\mathcal{E}_d=\int_0^\infty\left[\sin^2\omega+\left(\frac{d\omega}{dt}\right)^2\right]t\,dt, \tag{37}$$

$$\mathcal{M}=2\int_0^\infty(1+\cos\omega)\,t\,dt. \tag{38}$$

The Euler differential equation which minimizes this total energy is

$$\frac{1}{t}\frac{d}{dt}\left(t\frac{d\omega}{dt}\right)-\frac{1}{2}\sin(2\omega)-h\sin\omega=0, \tag{39}$$

with the same boundary condition as in Eq. (12) at $t=\infty$.

It should be noted that in the curling mode studied in Ref. 9 the differential equation is nearly, but not exactly the same as in Eq. (39) here. The main difference is in the exchange energy, which gives rise to a $t^{-2}\sin(2\omega)$ term in the differential equation for the curling. This term enforces a boundary condition $\omega=0$ or π at $t=0$ for the curling, instead of $\omega'=0$ at $t=0$ for the present, rotational mode, which turns out to make a large difference in the result. The scale of t and h is also different in this case, but it does not affect the solution, which depends only on the mathematical form.

B. Numerical integration

The integration of Eq. (39) is similar to that of Eq. (11), and it is also convenient to start it from large values of t, for which the behavior can be expressed by the eigenfunctions of a *linear* differential equation. However, these eigenfunctions are not as easy to handle as those of the spherical nucleation center, and we did not use the full possibilities of Eq. (13) as in that case. We consider only the start, for large t, and substitute the relation

$$\omega=\pi-\epsilon \tag{40}$$

in Eq. (39). To a first order in ϵ,

$$\frac{1}{t}\frac{d}{dt}\left(t\frac{d\epsilon}{dt}\right)=(1-h)\epsilon. \tag{41}$$

The solution which is regular at infinity of Eq. (41) is

$$\epsilon=b^*K_0(t\sqrt{1-h}), \tag{42}$$

where b^* is a constant, and K_0 is the modified Bessel function of the third kind. These functions *can* be handled,[10] but not as easily as the exponential functions encountered in the foregoing, for the spherical nucleus. Therefore we have linearized the equation in this cylindrical case only for the vicinity of $\omega=\pi$, namely for large t. In this region, when the argument is sufficiently large, we replace the Bessel function by its asymptotic value,[11] and use just

$$\epsilon=b\,e^{-t\sqrt{1-h}}/\sqrt{t}. \tag{43}$$

The strategy of the solution was the same as in Sec. II B, but in this case we used only a transformation of the differential equation to a difference equation. The contribution of the region $t\geq T$ was calculated similarly to Eqs. (18) and (19), and gave exactly the same expression as in Eq. (18) for $\mathcal{M}_L$, and

$$\begin{aligned}\mathcal{E}_{d_L}&=\frac{1}{4}\int_T^\infty t\left[\left(\frac{d\omega}{dt}\right)^2+\sin^2\omega\right]dt\\&\approx\frac{b^2}{4}\int_T^\infty\left(2-h+\frac{\sqrt{1-h}}{t}+\frac{1}{4t^2}\right)e^{-2t\sqrt{1-h}}dt\\&=\frac{b^2}{8}\left[\left(\frac{1}{2T}+\frac{2-h}{\sqrt{1-h}}\right)e^{-2T\sqrt{1-h}}+E\right],\end{aligned} \tag{44}$$

with

$$E = \sqrt{1-h}\int_T^\infty \frac{e^{-2t\sqrt{1-h}}}{t}\,dt. \tag{45}$$

We approximated this term by the first three terms of the expansion in Ref. 12. Its contribution to the total energy was very small in all cases, and the inaccuracy in its evaluation was negligible.

IV. RESULTS

A. Sphere

Results of the numerical integration of Eq. (11) are plotted in Fig. 1 for various values of h. For rather large h the integration was straightforward, but it became more tedious with decreasing h. The reason is quite obvious from Fig. 1, which shows a high slope, almost an abrupt change, for the smaller values of h. This high slope requires more accuracy than is necessary for larger values of h. It also requires very large values of the initial parameter b in Eq. (16a), and becomes very sensitive to the initial choice of that parameter.

However, for a very small h it is quite clear that the obtained magnetization structure approaches asymptotically the phenomenological model where the nucleation center becomes essentially a large sphere saturated along the z direction, which is surrounded by a rather sharp domain wall, the outside of which is saturated along $-z$. It is the picture postulated in Ref. 13, but it should be noted that a factor of 2, needed to account for reversal, has been omitted from Eq. (3) of Ref. 13, so that the factor 64 in Eq. (4) of Ref. 13 is actually 16. Also, W of Ref. 13 is shown in the present study to vanish, and the applied field H_z in the present notation is to be identified with $H - 4\pi M/3$ of Ref. 13. Since there is no additional magnetostatic energy when $\mathbf{M}$ is a function of r only, as proved in the Appendix, the wall energy per unit area, σ, is a constant on the sphere, and can be taken as that of a planar (one-dimensional) Bloch wall, when the sphere radius, R_0, is large enough so that its curvature may be neglected over distances of the order of the wall thickness. The energy of this model is

$$W_p = 4\pi R_0^2\sigma - 2M_s H_z(4\pi/3)R_0^3, \tag{46}$$

where the second term is the interaction with the applied field, H_z. Normalizing to the reduced units used here, by dividing the energy by W_0 of Eq. (4), using the field as in Eq. (9), and the length as in Eq. (5), namely

$$T = R_0\sqrt{2K_u/C}, \tag{47}$$

Eq. (46) becomes

$$\mathcal{E}_p = \frac{W_p}{W_0} = \frac{\sigma T^2}{2\sqrt{2K_uC}} - \frac{hT^3}{3}. \tag{48}$$

Substituting the Bloch wall energy value[14]

$$\sigma = 2\sqrt{2K_uC}, \tag{49}$$

and equating to zero the derivative with respect to T,

$$T = 2/h. \tag{50}$$

Subsituting this value in Eq. (48), the total energy is

$$\mathcal{E}_p = 4/(3h^2) \tag{51}$$

and the integrated magnetization is

$$\mathcal{M}_p = 8/(3h^3). \tag{52}$$

It is possible to use this relation also for estimating b of Eq. (16a) for starting the computations from a large t. Since a Bloch wall centered at T can be written as

$$\tan(\omega/2) = e^{t-T}, \tag{53}$$

it may be approximated, for large t by

$$\omega = \pi - 2e^{T-t}, \tag{54}$$

where T is given by Eq. (50). Equating this to Eq. (16a) one obtains the following relation, which turned out to be a very good start for searching the numerical solution at some chosen (large) value of T:

$$b = 2t\,e^{T-t+t\sqrt{1-h}}. \tag{55}$$

Figure 2 plots the total reduced energy, $\mathcal{E}$ as computed from the magnetization structures of Fig. 1, and compares it with the phenomenological $\mathcal{E}_p$ of Eq. (51). The agreement for small h (namely $T \gg 1$) is seen to be satisfactory, so that it is not necessary to compute below the region shown. The figure also shows the numerical results for $h \geq 0.6$ on a larger scale.

Similar results for the integrated reduced magnetization, $\mathcal{M}$, are shown in Fig. 3 and compared with the phenomenological $\mathcal{M}_p$ of Eq. (52). In this case the agreement is much better than in Fig. 2, and extends to $h = 0.5$, and even larger. It is still quite a good approximation even

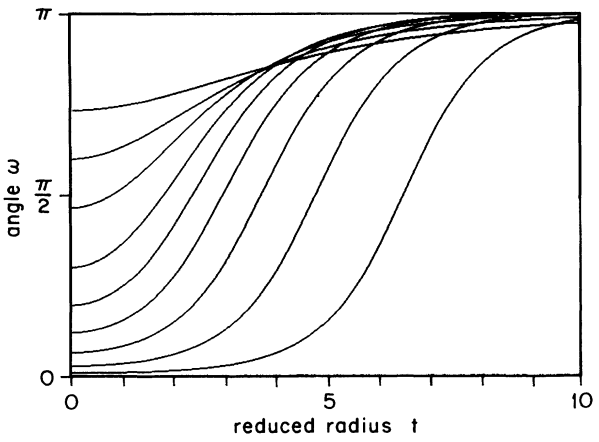

FIG. 1. The magnetization structure in the spherical reversal nucleus as obtained from the numerical integration of the Euler differential equation (11). The values of the reduced field, h, are (from the bottom to the top on the left-hand side) 0.3, 0.4, 0.5, 0.6, 0.7, 0.8, 0.9, 0.95, and 0.98.

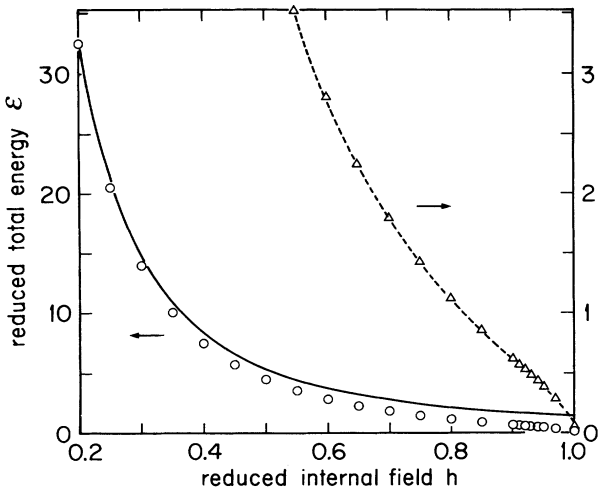

FIG. 2. The reduced total energy, $\mathcal{E}$, as computed from the solution of the Euler differential equation (11), given as points. The full line is the phenomenological approximation of Eq. (51). The points between the dashed line are plotted on the expanded scale on the right-hand side.

for $h = 0.9$, where the exact solution starts to *increase* with increasing h.

For the numbers plotted in Figs. 2 and 3 we have also computed

$$\delta = \mathcal{E}_d(h \pm \epsilon) - h\mathcal{M}(h \pm \epsilon) - [\mathcal{E}_d(h) - h\mathcal{M}(h)], \quad (56)$$

for different values of h and ϵ. We found this δ to be always a negative number, as was the case[1] for the planar walls. This negative value means that there are nearby configurations for which the energy is smaller than that of the computed configuration. In other words, the computed structure is a saddle point in configuration space. It is also interesting to note that $\mathcal{E}_d(h) - h'\mathcal{M}(h)$ was always negative for $h' > 1.1$. This result suggests that a range of small reversal nuclei may be the fastest reversal mechanism for an overcritical applied field.

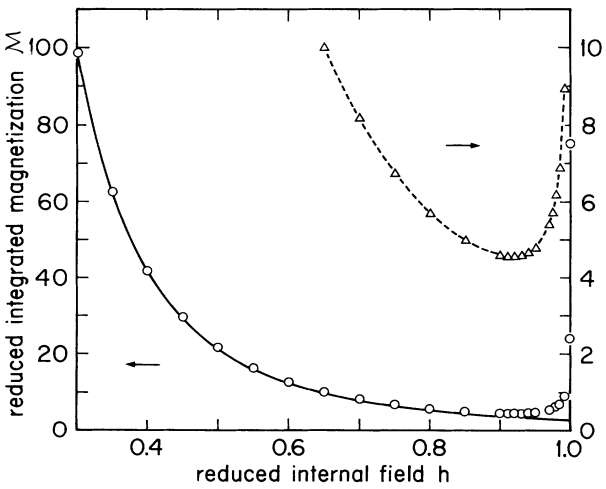

FIG. 3. The reduced integrated magnetization, $\mathcal{M}$, as computed from the solution of the Euler differential equation, given as points. The full line is the phenomenological approximation of Eq. (52). The points between the dashed lines are plotted on the expanded scale on the right-hand side.

Of course, finding a saddle point does not necessarily mean that it is the lowest possible saddle point. In this kind of a solution it is not possible to consider *all* configurations, and find the easiest route for going from $\omega = \pi$ to $\omega = 0$, as was done[15] in the rather simple case of an energy barrier which is made of an anisotropy energy only. In certain computer models the lowest energy barrier may be found numerically,[16] but even then it is usually restricted to certain imposed modes. In the present calculations, the study is restricted to a spherical symmetry, and it is not clear if the reversal may not be easier when an angular dependence is allowed. In this respect, the energy barrier computed here is only an upper bound to the best route, or the easiest mode of reversal. Therefore, any switching time calculated from it will also be only an upper bound to the lowest possible switching time.

Nevertheless, such a time estimation from the present results will at least be realistic, unlike the wild guesses found in the literature. For example, in a recent publication[17] the energy barrier is taken as the difference between the saturated states before and after magnetization reversal, while the reversal time is estimated from the arbitrary assumption that the reversal is "initiated in an activation volume V," in spite of the proof[4] that such a mechanism is ruled out by the exchange interaction on the border of the "activation volume." It should be noted that quite large volumes are involved in the solution reported here.

The energy we obtain is also quite large, even when it does not tend to infinity at very small h. The total energy we find for $h = 0.95$ is $0.38W_0$, which is 1.37×10^{-11} erg for cobalt, or one order of magnitude larger than the estimated[4] barrier, which can be overcome by thermal agitation, within an experimental time of 10^2 sec, at room temperature.

B. Cylinder

Results of the numerical integration of Eq. (39) are plotted in Fig. 4 for various values of h. Qualitatively, these results look very much the same as Fig. 1, and the whole computation was quite similar to that described in the foregoing. In particular, for rather large h the integration was straightforward, but it became more and more tedious and time consuming with decreasing h. Therefore, for this case as well we tried the asymptotic picture of a saturated cylinder, surrounded by a wall which separates it from an outer cylinder, saturated in the opposite direction. This picture, which should be valid for a small h, yields an energy per unit length,

$$W_p = 2\pi R_0 \sigma_N - 2M_s H_z \pi R_0^2, \quad (57)$$

where σ_N is the energy per unit area of a Néel wall. Normalizing to the reduced energy and field units used

here, and normalizing the length as

$$T = R_0\sqrt{2(K_u + \pi M_s^2)/C}, \tag{58}$$

Eq. (57) becomes

$$\mathcal{E}_p = W_p/(\pi C) = 4T - 2T^2h. \tag{59}$$

Equating to zero the derivative with respect to T,

$$T = 1/h. \tag{60}$$

Subsituting this value in Eq. (59), the total energy is

$$\mathcal{E}_p = 2/h \tag{61}$$

and the integrated magnetization is

$$\mathcal{M}_p = 2/h^2. \tag{62}$$

Figure 5 plots the total reduced energy $\mathcal{E}$, as computed from the magnetization structures of Fig. 4, and compares it with the phenomenological $\mathcal{E}_p$ of Eq. (61). It is obvious that the lines approach each other asymptotically for $h \rightarrow 0$, but in the region shown, the agreement is not nearly as good as in the case of the spherical nucleus. The same can be said about the results for the integrated reduced magnetization, $\mathcal{M}$, plotted in Fig. 6 and compared with the phenomenological $\mathcal{M}_p$ of Eq. (62). Both figures also show the numerical results for the larger h on an expanded scale.

It is not quite clear if the energy of the present mode is larger or smaller than that of the curling mode, as computed in Ref. 9, because the published numerical results for the latter mode are for the case $Q = 0$ only. It is also not easy to estimate *a priori* which is larger, because there are two competing effects. On the one hand, the curling mode has an extra exchange energy term, which does not exist in the present mode. On the other hand, the curling is constrained to $\omega = 0$ at $t = 0$, which does not allow the central cylinder to grow as much as it does in our mode, and this smaller reversal nucleus *may* involve a smaller total energy.

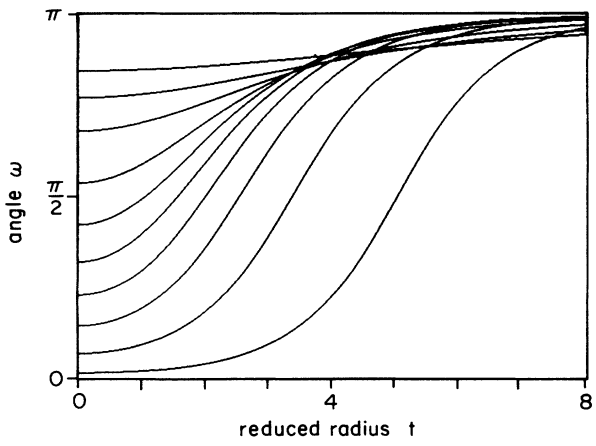

FIG. 4. The magnetization structure in the cylindrical reversal nucleus as obtained from the numerical integration of the Euler differential equation (39). The values of the reduced field, h, are (from the bottom to the top on the left-hand side) 0.2, 0.3, 0.4, 0.5, 0.6, 0.7, 0.8, 0.9, 0.95, and 0.98.

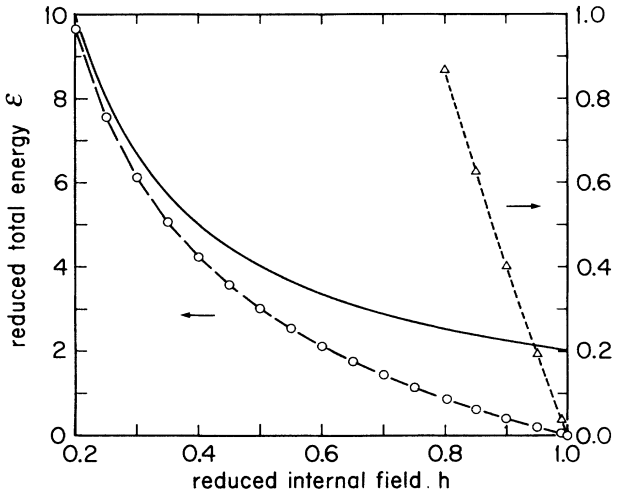

FIG. 5. The reduced total energy, $\mathcal{E}$, as computed from the solution of the Euler differential equation (39), given as points. The dashed line connecting the points is only meant to guide the eye. The full line is the phenomenological approximation of Eq. (61). The points between the dotted lines are plotted on the expanded scale on the right-hand side.

APPENDIX: MAGNETOSTATIC ENERGY

In spherical coordinates, the direction cosines of the magnetization vector expressed by Eq. (1) are

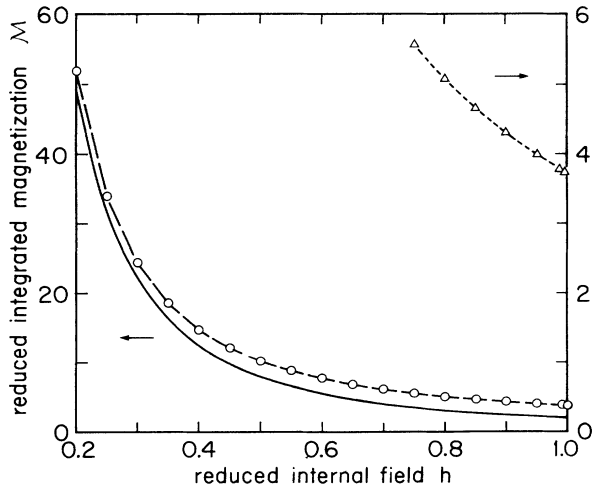

FIG. 6. The reduced integrated magnetization, $\mathcal{M}$, as computed from the solution of the Euler differential equation, given as points. The dashed line connecting the points is only meant to guide the eye. The full line is the phenomenological approximation of Eq. (62). The points between the dotted lines are plotted on the expanded scale on the right-hand side.

$$\alpha_r = \sin\omega(r)\sin\theta\cos\phi + \cos\omega(r)\cos\theta, \quad \text{(A1a)}$$

$$\alpha_\theta = \sin\omega(r)\cos\theta\cos\phi - \cos\omega(r)\sin\theta, \quad \text{(A1b)}$$

$$\alpha_\phi = -\sin\omega(r)\sin\phi, \quad \text{(A1c)}$$

which may be supplemented by

$$\alpha_\rho = \sin\omega(r)\cos\phi. \quad \text{(A1d)}$$

Substituting these relations in Eqs. (7) and (8) of Ref. 18, and carrying out the integrations over the angles ϕ and ϕ',

$$\frac{W_M}{2\pi^2 M_s^2} = \int_0^R \int_0^\pi r^2 g(r,\theta)\sin\theta\, d\theta\, dr - \frac{1}{2}\sum_{n=1}^{\infty}\sum_{m=\pm1}\frac{(n-m)!}{(n+m)!}\Omega_{mn}\int_0^R \frac{\sin\omega(r)}{r^n}\int_0^r (r')^{n+1}\sin\omega(r')\, dr'\, dr, \quad \text{(A2)}$$

since all the terms containing either $\cos\omega(r)$ or $\cos\omega(r')$ which do not vanish because of the integration over either ϕ or ϕ' are readily seen to be proportional to

$$\int_0^\pi P_{n+1}(\cos\theta)\sin\theta\, d\theta,$$

which is zero. Here

$$g(r,\theta) = \sin^2\omega\sin^2\theta + 2\cos^2\omega\cos^2\theta \quad \text{(A3)}$$

$$\Omega_{mn} = \int_0^\pi f_1(\theta)\, d\theta \int_0^\pi f_2(\theta')\, d\theta', \quad \text{(A4)}$$

$$f_1(\theta) = (n-m+1)\cos\theta P_{n+1}^m(\cos\theta) - nP_n^m(\cos\theta), \quad \text{(A5)}$$

$$f_2(\theta') = (n+m)\cos\theta' P_{n-1}^m(\cos\theta') - (n+1)P_n^m(\cos\theta'). \quad \text{(A6)}$$

Now, it can be seen from the rules of differentiating the Legendre functions that

$$\frac{d}{d\theta}\left[\sin\theta P_{n-1}^1(\cos\theta)\right] = (1-n)\left[\cos\theta P_{n-1}^1 - P_n^1\right]. \quad \text{(A7)}$$

By integrating this equation between 0 and π, it is seen that the integral of f_2 vanishes for $n > 1$ and $m = 1$. The same applies to $m = -1$, because

$$n(n+1)P_n^{-1}(\cos\theta) = P_n^1(\cos\theta), \quad \text{(A8)}$$

so that Ω_{mn} may at most be nonzero for $n = 1$. However, for $n = 1$ the function f_1 is proportional to $(3\cos^2\theta - 1)\sin\theta$, which also integrates to zero.

It has thus been shown that only the first term of Eq. (A2) need to be considered. Using Eq. (A3) in this term, and integrating over θ, the result is

$$W_M = \frac{8}{3}\pi^2 M_s^2 \int_0^R r^2 dr, \quad \text{(A9)}$$

which is independent of ω. It is also the same as the magnetostatic self-energy of a *saturated* sphere.

For a phenomenological understanding of the result, consider first two concentric spheres, whose radii are R_1 and R_2. If the region between the R_1 and R_2 is magnetized homogeneously, the field due to the charge on R_1 cancels that due to the charge on R_2, and the hollow region $r < R_1$ is field free. Therefore, the magnetization of another hollow sphere inserted in that space can be rotated without doing any work. One can then imagine a whole series of concentric spheres whose magnetization is rotated at some different angles with respect to each other, and the effect of the volume charge created in this way still cancels the effect of the charge on the outer surface, R_2, so that the total energy is still the same as that of the homogenenously magnetized, saturated sphere.

*Permanent address: Department of Electronics, Weizmann Institute of Science, 76100 Rehovoth, Israel.

[1] J. S. Broz, H. B. Braun, O. Brodbeck, W. Baltensperger, and J. S. Helman, Phys. Rev. Lett. **65**, 787 (1990).
[2] Hans-Benjamin Braun, IEEE Trans. Magn. **27**, 4787 (1991).
[3] C. H. Stapper, Jr., J. Appl. Phys. **40**, 798 (1968).
[4] A. Aharoni, J. Appl. Phys. **33**, 1324 (1962).
[5] A. Aharoni, Rev. Mod. Phys. **34**, 227 (1962).
[6] Amikam Aharoni, IEEE Trans. Magn. **27**, 4775 (1991).
[7] A. Aharoni, J. Appl. Phys. **30**, 70S (1959).
[8] A. Aharoni, Phys. Status Solidi **16**, 3 (1966).
[9] J. S. Broz, Ph.D. thesis, Eidgenossische Technische Hochschule, 1991 (unpublished); J. S. Broz and W. Baltensperger, Phys. Rev. B **45**, 7307 (1992).
[10] A. Aharoni, J. Comput. Phys. **4**, 270 (1969).
[11] I. S. Gradshteyn and I. M. Ryzhik, *Table of Integrals, Series and Products* (Academic, New York, 1965), Eq. 8.451.6.
[12] I. S. Gradshteyn and I. M. Ryzhik, *Table of Integrals, Series and Products* (Academic, New York, 1965), Eq. 8.215.
[13] W. Baltensperger, J. S. Broz, and J. S. Helman, Mod. Phys. Lett. B **5**, 1061 (1991).
[14] F. H. de Leeuw, R. van den Doel, and U. Enz, Rep. Prog. Phys. **43**, 690 (1980), Eq. (2.26).
[15] I. Eisenstein and A. Aharoni, Phys. Rev. B **14**, 2078 (1976).
[16] A. Lyberatos and R. W. Chantrell, IEEE Trans. Magn. **MAG-26**, 2119 (1990)
[17] Y. Otani, H. Myajima, T. Kubodera, and S. Chikazumi, IEEE Trans. Magn. **MAG-26**, 1742 (1990).
[18] A. Aharoni, J. Appl. Phys. **51**, 5906 (1980).